A Platinum Open Access Journal for Organic Chemistry

Paper

Free to Authors and Readers | DOAJ Seal | *Arkivoc* **2023** (ii) 202311998

Synthesis, solid-state structure, and electrochemical properties of thienodipyrimidine-2,4,5,7-tetra(thi)ones

Anna I. Wright, Benson M. Kariuki, and Yi-Lin Wu*

School of Chemistry, Cardiff University, Main Building, Park Place, Cardiff CF10 3AT, United Kingdom
Email: WuYL@cardiff.ac.uk

Dedicated to Professor Tien-Yau Luh on the occasion of his 76th birthday

Received 04-02-2023 **Accepted Manuscript** 06-18-2023 **Published on line** 07-21-2023

Abstract

Thienodipyrimidine-2,4,5,7-tetra(thi)ones were prepared by one-pot photocyclization from barbituric acid derivatives. The structures of these tricyclic molecules with multiple (thio)carbonyl groups were determined by NMR and single-crystal X-ray diffraction analysis, and the electrochemical properties were studied by cyclic voltammetry and DFT calculations. The solid-state structures of these molecules feature dipolar C=S (or C=O), chalcogen-bonding, and π-stacking interactions. The presence of two adjacent thiocarbonyl groups allows for a two-center three-electron (2c/3e) interaction upon oxidation, significantly lowering the oxidation potential.

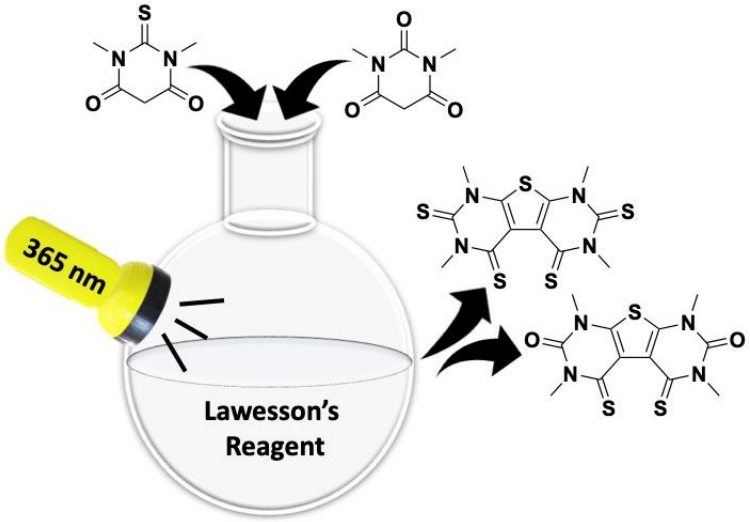

Keywords: Photocyclization, electrochemistry, chalcogen bond, two-center three-electron bond.

Introduction

Recent advances have been made in developing air-stable organic field-effect transistors (OFETs) for their potential application in flexible, lightweight, and low-cost electronic devices.[1–3] Incorporation of sulfur atoms into the molecular skeleton gives rise to a promising class of high-performance organic transistors.[4–6] Particularly, it has been demonstrated that thiocarbonyl functionalization enhances intermolecular interactions due to the presence of S-S interactions, and improves the transport properties of the molecule.[7–9] The larger or more diffused sulfur orbitals form close contacts with neighboring molecules, favoring highly ordered and closely packed structures.[8,10,11] Subsequently, the S-S interactions in OFETs have been noted for their sufficiently stable performance in air, due to the stabilized lowest unoccupied molecular orbital (LUMO) and improved electron mobility.[3,12,13] However, this promising design motif has yet to be fully exploited for OFETs in molecules other than birhodanine or rylene dye derivatives.[1,13-15]

In our continuous study of thiocarbonyl derivatives for photosensitization,[16–18] we serendipitously discovered that thionating barbituric acid derivatives resulted in the formation of thienodipyrimidine-2,4,5,7-tetrathiones (**1**, Figure 1). Similar to birhodanine derivatives, this redox-active tricyclic molecule features a medium-sized π-surface, multiple C=S units, and rich intermolecular interactions, which should be tunable by replacing some of the sulfur atoms with oxygen. Inspired by the potential of birhodanines for OFET applications and the reported photocatalytic ability of pyrimidopteridine tetraone[15,19,20] (an analogous compound with a pyrazino central ring), we report here the synthesis of thienodipyrimidine-2,4,5,7-tetra(thi)ones **1**–**4** (Figure 1) and their electrochemical properties.

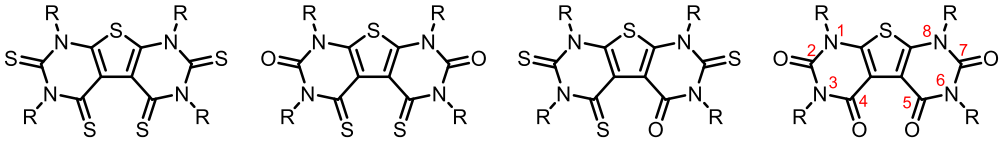

Figure 1. Structures of thienodipyrimidine-2,4,5,7-tetrathione and the oxo-analogous **1-S$_4$**, **2-O$_2$S$_2$**, **3-OS$_3$**, and **4-O$_4$**. The ring-skeletal numbering following the IUPAC convention is provided.

Results and Discussion

With the aim of investigating the photophysical properties of barbituric acid chromophores with varying degrees of thionation, *N,N'*-dimethyl-2-thiobarbituric acid was treated with Lawesson's reagent,[21] which unexpectedly yielded **5** (4%) and **1a-S$_4$** (4%; Scheme 1). Structural determination of both molecules was supported by ^{1}H and ^{13}C NMR spectroscopy, high-resolution mass spectrometry, and single-crystal X-ray diffraction (see later for discussion). Following this discovery, the reaction conditions were then varied to improve the yield of **1a-S$_4$** (Table 1); under a normal atmosphere, the yield of **1a-S$_4$** increased with increasing equivalents of Lawesson's reagent and the reaction time (entries 1–3, 4–44%). When the reaction was conducted in CH_2Cl_2 at reflux, **1a-S$_4$** was not detected after 24 h (entry 4), suggesting high temperatures are required for thionating barbituric acid. Finally, various irradiation sources were implemented under either an aerated or N_2 atmosphere to determine whether irradiation is necessary for the cyclization process (entries 5–10). UV irradiation (365 nm LED) in the presence of oxygen yielded **1a-S$_4$** in the highest yield (44%, entry 7), indicating that either natural or artificial UV

irradiation is essential to initiate the dimerization and cyclization processes. To ensure reproducible light exposure, the synthesis of other structural analogues was carried out under UV irradiation.

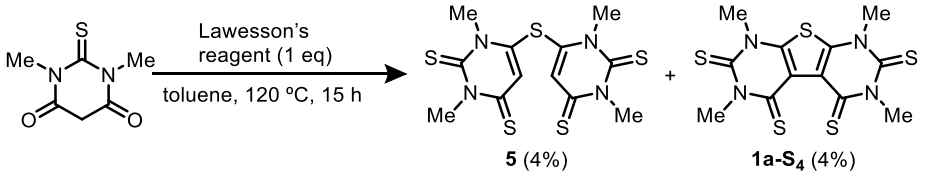

Scheme 1. Unexpected formation of **1a-S$_4$**.

Table 1. Optimization for **1a-S$_4$** synthesis[a]

Entry	Lawesson's reagent	Solvent	Time	Atmosphere	Light source	Yield (%)	
						1a-S$_4$	**5**
1	1.0 eq	Toluene	15 h	Air	Ambient	4	4
2	1.6 eq	Toluene	24 h	Air	Ambient	28	–
3	2.5 eq	Toluene	24 h	Air	Ambient	44	–
4	2.5 eq	CH_2Cl_2	24 h	Air	Ambient	0	–
5	2.5 eq	Toluene	24 h	Air	White light LED[b]	21	–
6	2.5 eq	Toluene	24 h	N_2	White light LED[b]	6	–
7	2.5 eq	Toluene	24 h	Air	UV LED[c]	44	–
8	2.5 eq	Toluene	24 h	N_2	UV LED[c]	10	–
9	2.5 eq	Toluene	24 h	Air	Dark	9	–
10	2.5 eq	Toluene	24 h	N_2	Dark	9	–

[a] A mixture of *N,N'*-dimethyl-2-thiobarbituric acid (100 mg, 0.58 mmol), Lawesson's reagent, and solvent (10 mL) was stirred at reflux for a specified time. The reaction was worked up according to the experimental procedure for **1a-S$_4$** (see the experimental section). [b] EvoluChem 6200K LED; λ_{irrad} 415–725 nm. [c] EvoluChem 365 PF LED; λ_{irrad} 355–385 nm.

Oxo analogues **2a**–**4a** can be prepared using *N,N'*-dimethylbarbituric acid as the starting material or through oxidative desulfurization[22,23] of suitable precursors (Scheme 2). Specifically, treating *N,N'*-dimethylbarbituric acid with Lawesson's reagent yielded compound **2a-O$_2$S$_2$**, with two urea-type C=O groups (i.e. 2,7-dioxo), along with **6** as a minor product. Compound **6** has been previously reported and it appears as a mercaptothione instead of a structurally symmetric dithione tautomer by NMR, in agreement with the literature.[22] Successive Cu-mediated oxidation of **1a-S$_4$** gave **3a-OS$_3$** and **4a-O$_4$** at room and high temperatures, respectively. Other oxo-isomers, such as 4,5-dioxo (found 341.01 *m/z* for $C_{12}H_{13}N_2O_2S_3^+$) and 2,4,5-trioxo (325.06 *m/z* for $C_{12}H_{13}N_2O_3S_2^+$) may have been generated according to mass spectrometry analysis; however, these compounds were not isolated. It is of interest to note that Senga and co-workers previously reported the synthesis of **4a-O$_4$** by thermolysis of [1,2,3]thiadiazolo[4,5-*d*]pyrimidine-5,7(4*H*,6*H*)-diones.[24]

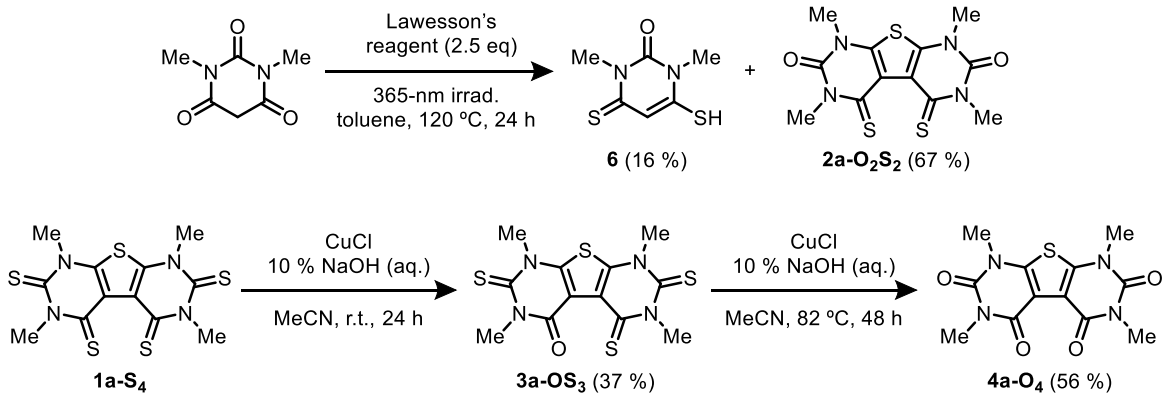

Scheme 2. Synthesis of **6**, **2a-O_2S_2**, **3a-OS_3**, and **4a-O_4.**

Ethyl analogues **1b-S_4**, **2b-O_2S_2**, and **3b-OS_3** were also prepared using similar reaction conditions. The ethyl analogue of **6** was observed by mass spectrometry (219.0244 *m/z* for $C_8H_{12}N_2OS_2^+$), but could not be isolated. The yield for each ethyl-substituted thienodipyrimidine tetra(thi)one is generally lower than that for the methyl derivatives, and **4b-O_4** could not be obtained (see experimental), highlighting the reduced reactivity affected by bulkier ethyl substituents.

Compounds **5** and **6** are likely intermediates in the course of **1** and **2** formation. The observation of these species suggests a one-pot, two-step mechanism shown in Scheme 3. In the first step, mercaptothione intermediate **A**, produced through thionation of the barbituric precursor with Lawesson's reagent, reacts with its dithione tautomer **A'** to give thioether **B** upon elimination of H_2S.[21,25,26] This reaction may proceed through a photochemical (upper pathway in Step 1) or thermal (lower pathway) route. In the photochemical route, the photoexcited **A'** abstracts a hydrogen atom from the thiol group of **A**;[25,27,28] the two radicals then combine to form the thioether linkage. As negligible **5** was observed in the dark reactions (Table 1, entries 9 and 10), this putative photochemical route may be significant. Notably, when *N,N'*-dimethylbarbituric acid was used as the starting material, thionation does not occur at the urea-like C=O group, indicating a substantial energy barrier for thionation at this position. Trace water in the solvent or the activated methylene group of barbituric acid provides a proton source for tautomerization. As light irradiation and an aerated atmosphere facilitate the formation of **1**, it is believed that photon absorption of **B** initiates cyclization to give **C**, which then undergoes air oxidation to afford the aromatic thieno unit in **1** and **2** (Scheme 3, step 2). This oxidative photocyclization is akin to the reported thiophene synthesis from aryl vinyl sulfides or divinyl sulfides.[29–32]

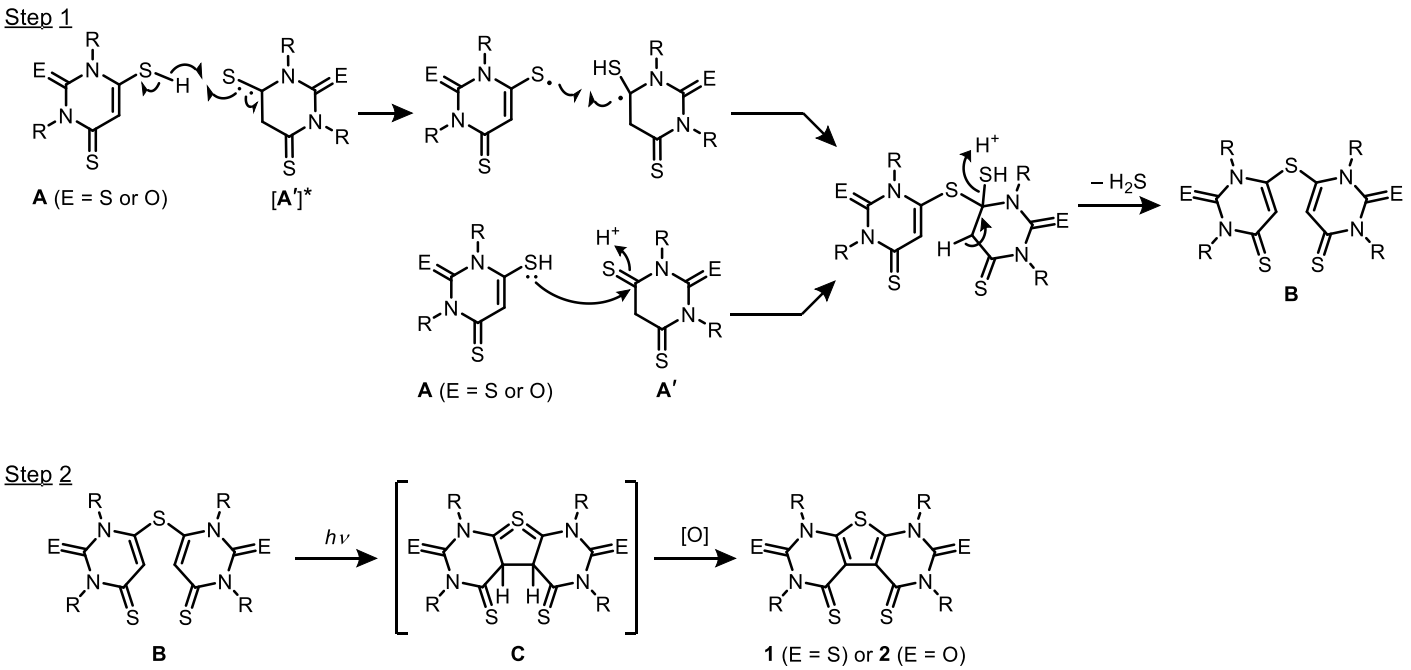

Scheme 3. A plausible mechanism for the formation of thioether and thienodipyrimidine-2,4,5,7-tetra(thi)one.

Crystals of **1**–**4** with suitable qualities for X-ray diffraction analysis were obtained by solvent diffusion or slow evaporation (see experimental details for crystallization methods). Compounds **1a/b-S$_4$** (crystallized in *Pc* and *Pbca*, respectively), **2a-O$_2$S$_2$** (*Pca*2$_1$), and **3a-OS$_3$** (*P*2$_1$/n), with at least one sulfur atom on the 4 or 5 position of thienodipyrimidine, display a twisted geometry; large dihedral angles θ(E4-C4-C5-S5) in the range 32–63° were observed (E = S or O, Table 2). In the absence of C=S groups, tetraone **4a-O$_4$** is nearly planar, with a small θ(O4-C4-C5-O5) of about 2°. Therefore, the non-planar, helicene-like structure of **1**–**3** should be caused by the steric congestion between the large chalcogen atoms in the 4/5 bay region.

Table 2. Structural feature of **1–4** by single-crystal X-ray analysis[a]

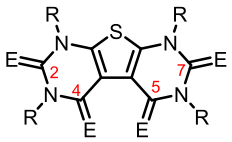

	θ(E4-C4-C5-E5) (°)	d(E4···E5) (Å)
1a-S$_4$	60.6	3.30
1b-S$_4$	62.7	3.32
2a-O$_2$S$_2$	53.2	3.19
3a-OS$_3$	32.8	2.87
4a-O$_4$	2.27	2.76

[a] Average value reported if crystallographically non-equivalent molecules present

The small size of the methyl substituent and a large number of chalcogen atoms in **1a**–**4a** permit various intermolecular short contacts. In the herringbone packing of **1a-S$_4$**, one C=S group on the 2/7 position forms

orthogonal interactions with a 2/7 C=S group of a neighboring molecule (d(S···C=S) = 3.32 Å and φ(S···C=S) = 82.5°; Figures 2a and 2b).[33,34] On the other hand, one C=S group on the 4/5 position is in short contact with the thiophene S (d(S···S) = 3.55 Å), indicative of chalcogen bonding between lone-pair electrons of thione C=S and $\sigma^*_{C\text{-}S}$ orbital of the thiophene unit.[35] Within each columnar stack of **1a-S$_4$**, the molecules are spaced by about 3.68 Å from each other. **2a-O$_2$S$_2$** also observes herringbone packing, with similar orthogonal interactions between the 2/7 C=O groups of neighboring molecules (d(O···C=O) = 3.12 Å and φ(O···C=O) = 87.7°; Figure 2c) and molecular stacking distances (3.51 Å); no chalcogen-bond-type interaction is observed. Ethyl-substituted **1b-S$_4$** similarly exhibits a herringbone-like packing; however, the distance between the orthogonal 2/7 C=S groups of neighboring molecules is longer than the sum of the van der Waals radii of S and C (d(S···C=S) = 3.62 Å; Figure 2d). Additionally, the presence of ethyl groups increases the intermolecular distances between both the C=S and thiophene S and the π-stacking molecules (~4 Å); therefore, it may be assumed that **1b-S$_4$** would exhibit poor electron mobilities and air-stability owing to the negligible intermolecular interactions.

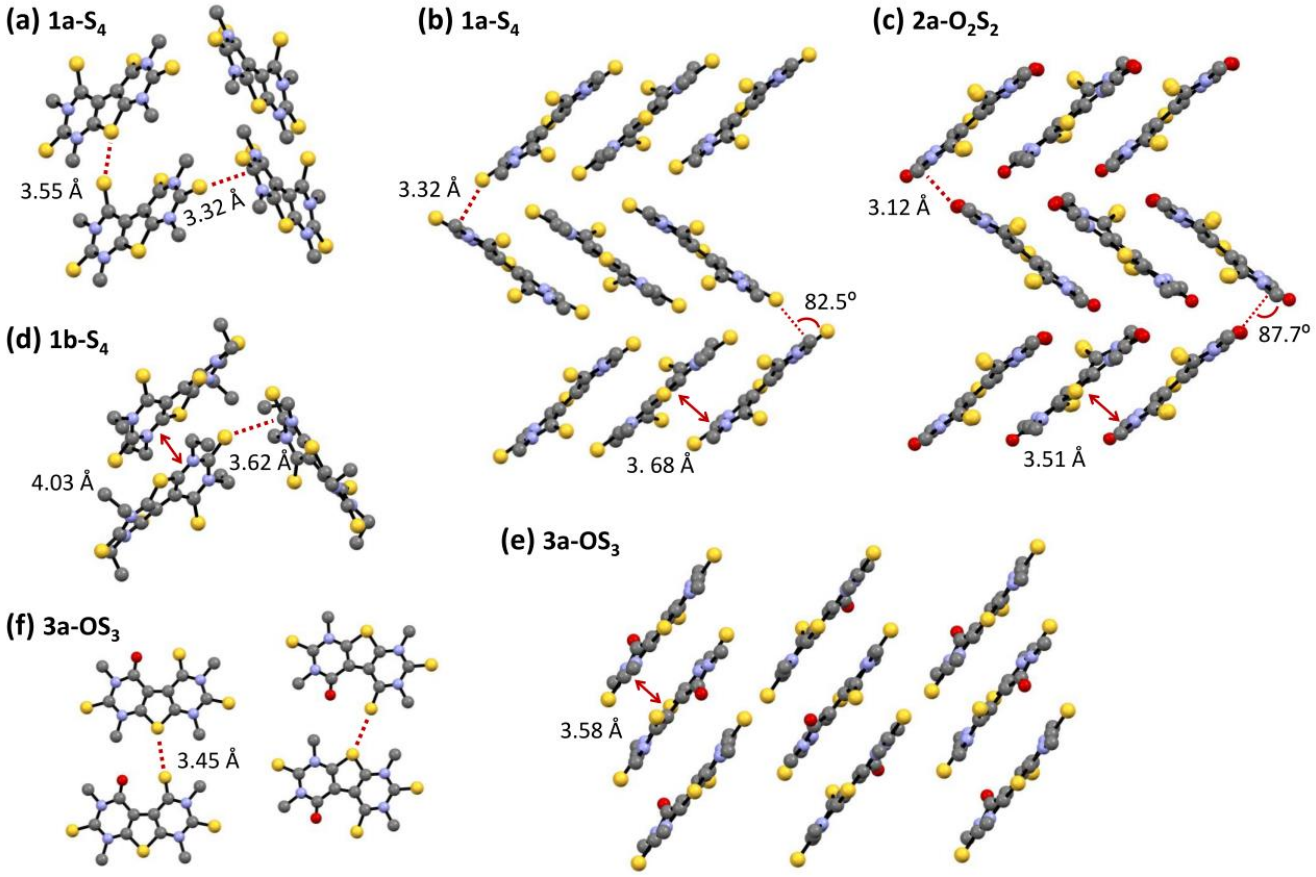

Figure 2. Single-crystal X-ray structures of **1a-S$_4$** (a and b), **2a-O$_2$S$_2$** (c), **1b-S$_4$** (d), and **3a-OS$_3$** (e and f). Panels (b), (c), and (e) show the molecular packing in **1a-S$_4$**, **2a-O$_2$S$_2$**, and **3a-OS$_3$**, respectively. Atoms color code: C grey, N blue, O red, S yellow. Hydrogen atoms are omitted for clarity.

The solid of **3a-OS$_3$** instead shows sheet-like packing, with small intermolecular spacing (3.58 Å; Figure 2e). Such a sheet arrangement is incompatible with forming orthogonal interactions between the 2/7 C=S groups of neighboring molecules. The distance between the C=S group on the 5 position and the thiophene S (d(S···S) = 3.45 Å; Figure 2f) is shorter than the chalcogen bonds observed for **1a-S$_4$**. We note that the C=S group acts as

the chalcogen bond acceptor in **3a-OS$_3$** rather than the C=O group. This observation contradicts the common expectation, given a more substantial negative charge on C=O's oxygen but highlights the potential for C=S to engage in non-covalent interactions.

The UV-Vis absorption spectra for thienodipyrimidine tetra(thi)ones **1**–**4** and thioether **5** in CH_2Cl_2 are shown in Figure 3 (Table 3). Each molecule shows absorption between 300–400 nm and no solvatochromic behavior was observed upon changing solvent polarity. The absorption intensity of the lower-energy band for each chromophore increases as the number of thiocarbonyls increases (~ 9 700 M^{-1} cm^{-1} per thionation). The shape of the absorption bands changes negligibly when the alkyl group is converted from methyl to ethyl groups. Thioether **5** absorbs strongly at 360 nm (ε = 36 410 M^{-1} cm^{-1}) in agreement with the 365 nm LEDs required to maximize the yield of **1a-S$_4$**.

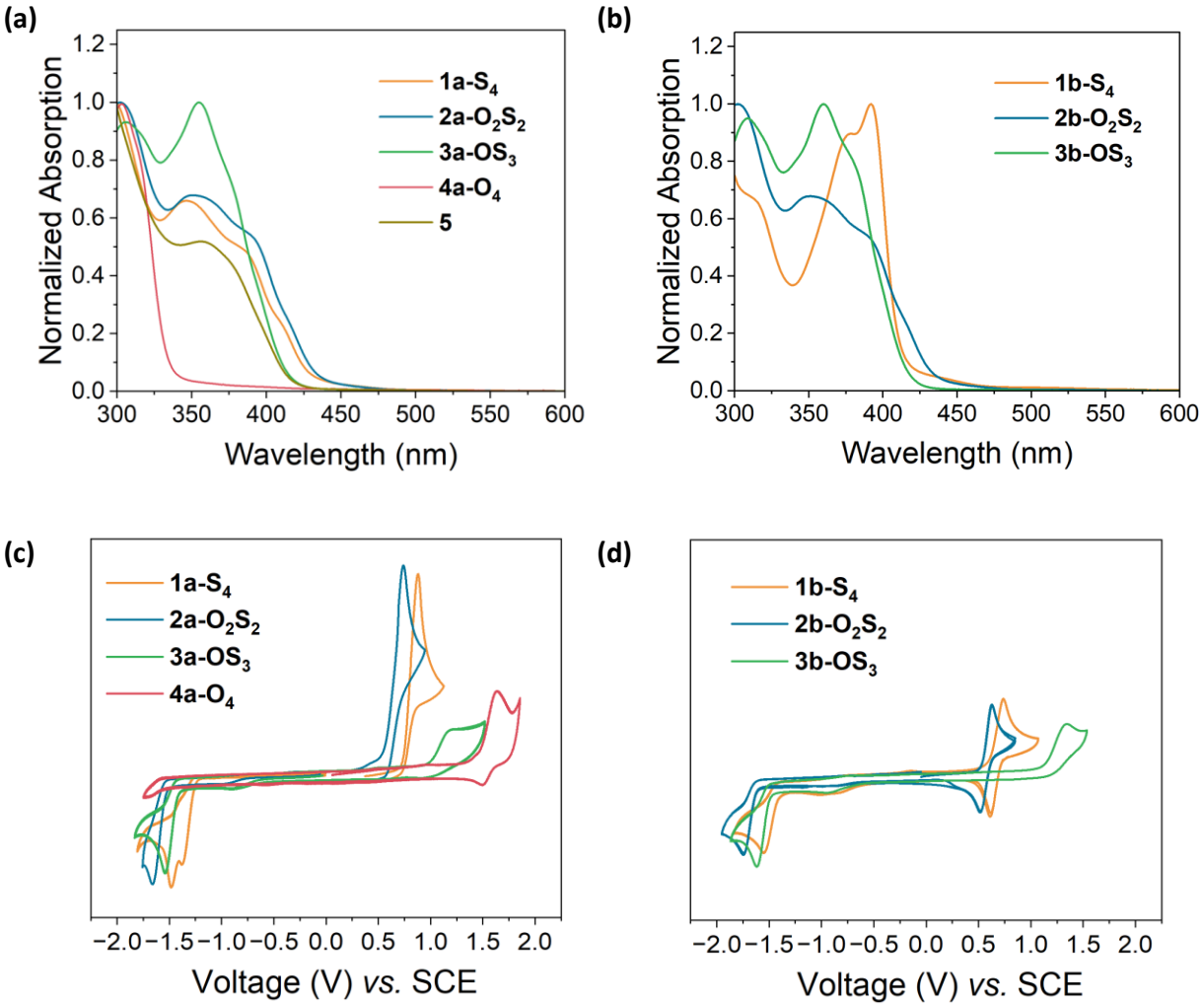

Figure 3. Normalized absorption spectra of (a) methyl and (b) ethyl thienodipyrimidine tetra(thi)ones in CH_2Cl_2; and cyclic voltammograms of (c) methyl and (b) ethyl thienodipyrimidine tetra(thi)ones in CH_2Cl_2 containing nBu$_4$NPF$_6$ (100 mM) as the supporting electrolyte with a scan rate of 100 mV s^{-1}.

Table 3. UV-Vis, electrochemical, and computed structural data of **1**–**4**

	λ_{abs}[a]	ε[a]	E_{OX}[b]	E_{RED}[b]	ΔG_{neu-ox}[c]	$\theta_{neutral}$[d]	$\theta_{oxidized}$[d]	$d_{neutral}$[e]	$d_{oxidized}$[e]
	(nm)	(M^{-1} cm^{-1})	(V *vs.* SCE)		(eV)	(°)		(Å)	
1a-S$_4$	385	24 305	0.85[f]	–1.36[f]	–5.45	64.07	32.70	3.43	2.67
	350	32 000		–1.47[f]					
2a-O$_2$S$_2$	390	14 685	0.70[f]	–1.68[f]	–5.21	63.08	21.17	3.44	2.69
	375	11 970							
3a-OS$_3$	355	25 920	1.22[f]	–1.52[f]	–6.10	49.67	50.51	3.13	3.07
4a-O$_4$	315	2 950	1.64[f]	< –2.00	–5.89	6.12	8.54	2.86	2.77
1b-S$_4$	390	15 960	0.63	–1.58[f]	–5.38	66.09	32.11	3.40	2.67
	355	19 980							
2b-O$_2$S$_2$	390	16 780	0.56	–1.72[f]	–5.18	64.46	28.17	3.41	2.68
	375	14 685							
3b-OS$_3$	380	22 550	1.32[f]	–1.62[f]	–6.09	48.89	49.26	3.09	3.03
	360	28 950							

[a] Molar extinction coefficients (ε) determined in CH_2Cl_2. [b] Redox potential $E = E_{1/2}$ determined by cyclic voltammetry in nBu$_4$NPF$_6$ (100 mM) in CH_2Cl_2. [c] Gibbs energy difference between the neutral and oxidized form, calculated at the (U-)ωB97X−D/6-31G(d,p) level of theory, with PCM solvation in CH_2Cl_2.[36] [d] Computed dihedral angle θ(E4-C4-C5-E5) as defined in Table 2. [e] Computed distance d(E4···E5) as defined in Table 2. [f] Irreversible peak potential.

The electrochemical properties of **1**–**4** are summarized in Table 3 and the cyclic voltammograms shown in Figure 3. The reduction potentials become more positive as the degree of thionation increases, indicating that thionation of a carbonyl molecule makes it a better electron acceptor, as discussed in our recent study.[37] Although the number of C=S (and hence C=O) units in **3-OS$_3$** is between that in **1-S$_4$** and **2-O$_2$S$_2$**, the oxidation potentials for **3-OS$_3$** are higher than those for **1-S$_4$** or **2-O$_2$S$_2$**. This surprising observation is in line with the much larger energy difference (ΔG_{neu-ox}) between the neutral and the 1-e$^-$ oxidized forms of **3-OS$_3$** in comparison to **1-S$_4$** or **2-O$_2$S$_2$**, computed at the (U-)ωB97X−D/6-31G(d,p) level of theory (Table 3). These results indicate that the oxidation potential is governed by the heteroatom composition on the 4 and 5 positions.

A closer examination of the optimized molecular geometry offers a clue for the explanation. Similar to the twisted structures found in the solid-state X-ray structure, the computed geometry shows a large dihedral angle θ(S4-C4-C5-S5) ~ 64° for **1-S$_4$** and **2-O$_2$S$_2$** and a slightly smaller one θ(O4-C4-C5-S5) ~ 50° for **3-OS$_3$**, due to the presence of large sulfur atoms. The deviation between the corresponding values in Tables 2 and 3 is likely a consequence of packing effects. However, upon 1-e$^-$ oxidation, the dihedral angle for radical cation **1-S$_4$**$^{\bullet+}$ and **2-O$_2$S$_2$**$^{\bullet+}$ reduced substantially to θ(S4-C4-C5-S5) ~ 30° whereas that for radical cation **3-OS$_3$**$^{\bullet+}$ remain at θ(O4-C4-C5-S5) ~ 50° (a minor change was also found for **4-O$_4$**$^{\bullet+}$). The reduction in the dihedral angle also manifests in the shortening of the d(S4···S5) distance in **1-S$_4$**$^{\bullet+}$ and **2-O$_2$S$_2$**$^{\bullet+}$. The d(S4···S5) ~ 2.7 Å in these radical cations is, in fact, significantly shorter than the sum of van der Waals radius of two sulfur atoms (3.8 Å).[38]

The electron spin density plots of radical cations of **1a**–**4a** in Figure 4 reveal the localization of the unpaired electron between the S4 and S5 atoms of **1-S$_4$**$^{\bullet+}$ and **2-O$_2$S$_2$**$^{\bullet+}$; the distribution resembles a σ-type orbital interaction between S4 and S5. On the other hand, the spin density of **3-OS$_3$**$^{\bullet+}$ and **4-O$_4$**$^{\bullet+}$ spreads the entire molecule and is of π symmetry (see also Figure S2). The localization of the spin density and the small d(S4···S5) point at a two-center three-electron (2c/3e) bonding interaction between the thiocarbonyl units on the 4 and 5

position (-C=S∴S=C-), a phenomenon that was reported for intermolecular systems.[39–41] In other words, the 2c/3e hemi-bonding between the two adjacent thiocarbonyl groups provides a stabilizing interaction[42] in the radical cation form of **1-S$_4$** and **2-O$_2$S$_2$**, allowing 1-e$^-$ oxidation of these species to occur at a much milder potential than the other derivatives.

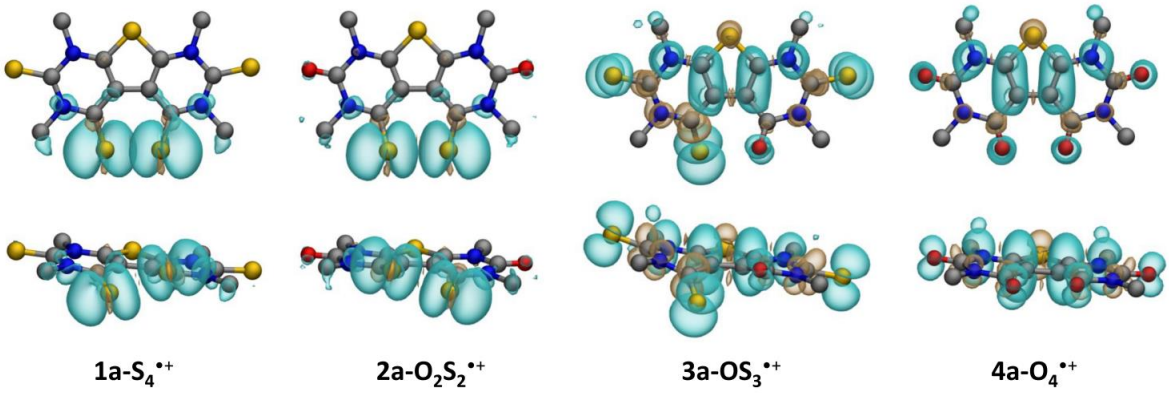

Figure 4. Electron spin density distributions (isosurface value 0.001 a.u.) for radical cations **1a-S$_4$**$^{\bullet+}$, **2a-O$_2$S$_2$**$^{\bullet+}$, **3a-OS$_3$**$^{\bullet+}$, and **4a-O$_4$**$^{\bullet+}$ calculated at UωB97X-D/6-31G(d,p) (with PCM solvation in CH_2Cl_2; top view above and side view below). Atoms color code: C grey, N blue, O red, and S yellow. Hydrogen atoms are omitted for clarity.

Conclusions

In summary, a series of thienodipyrimidine tetra(thi)ones have been synthesized *via* a one-pot photocyclization reaction of (2-thio)barbituric acid and successive Cu-mediated oxidation reactions. It was determined that both irradiation and aerated conditions are required for the cyclization process to occur. These molecules show photoabsorption mainly in the UV region and amphoteric electrochemical activities. In the presence of two C=S groups on the 4 and 5 positions, facile oxidation of these derivatives was observed, due to stabilizing intramolecular 2c/3e interaction in the radical cations. In the solid state, the molecular packing features dipolar C=S (or C=O), chalcogen-bonding, and π-stacking interactions, resulting in various short contacts between molecules. These favorable characteristics suggest the promising use of thienodipyrimidine tetra(thi)ones as field effect transistors. Our future study will identify which S-S interactions play a significant role in achieving air-stable transistors with superior electron mobilities.

Experimental Section

Materials and general methods. Materials were purchased at the reagent grade and used as received. Reactions were monitored by thin-layer chromatography using aluminium silica gel TLC plates; visualization was accomplished with UV light (254 nm or 366 nm). Flash column chromatography was carried out with SiO_2 (particle size 0.040–0.063 mm, 230–400 mesh) and technical solvents. Melting points were measured using a Stuart SMP11. ^{1}H and ^{13}C NMR spectra were measured on a Bruker AVANCE III HD 500 instrument. Chemical shifts were reported in ppm relative to the signal of $Si(CH_3)_4$ using the solvent residual signal as an internal reference ($CDCl_3$: δ_H = 7.26 ppm, δ_C = 77.16 ppm). Coupling constants (*J*) were given in Hz. The apparent

resonance multiplicity was described as s (singlet), d (doublet), t (triplet), q (quartet) and m (multiplet). Infrared spectra (IR) were recorded on a Shimadzu IR Affinity 1S FTIR spectrometer with a Specac Quest ATR accessory; vibration modes are reported in cm^{-1}. High-resolution mass spectra (HR-MS) were performed on a Waters LCT HR TOF mass spectrometer; signals are reported in *m/z* units.

Synthesis of 5 and 1a-S_4

A mixture of *N,N'*-dimethyl-2-thiobarbituric acid (300 mg, 1.74 mmol) and Lawesson's reagent (705 mg, 1.74 mmol) in toluene (30 mL) were stirred at reflux for 15 h. The reaction was then cooled to room temperature (r.t.), and the reaction mixture was washed with sat. $NaHCO_3$ (100 mL) and extracted with CH_2Cl_2. The organic layers were collected, dried over Na_2SO_4 and the solvent was removed under vacuum. The crude mixture was purified by silica gel chromatography (1:1 CH_2Cl_2:toluene) to give **5** (13 mg, 4%) yellow solid and **1a-S_4** (13 mg, 4%) as a red solid.

5: Suitable crystals for X-ray diffraction were grown by slow evaporation from $CHCl_3$; m.p. 213–216 °C; ^{1}H NMR (500 MHz, $CDCl_3$): δ_H 6.88 (s, 2H), 4.22 (s, 6H), 3.94 (s, 6H); ^{13}C NMR (126 MHz, $CDCl_3$): δ_C 184.7, 176.1, 138.9, 122.0, 44.2, 42.4. IR (ATR): $\tilde{\nu}$ = 3048 (w), 2918 (w), 1691 (w), 1577 (m, C=C), 1545 (m, C=C), 1458 (m), 1396 (m), 1275 (s, sh at 1320 cm^{-1}, ring motion involving C=S), 1192 (w), 1151 (w), 1064 (s), 966 (w), 865 (w), 798 (m), 756 (w), 663 (w) cm^{-1}; HR-MS (ES+): 374.9889 *m/z* ([*M* + H]$^+$), calcd for $C_{12}H_{15}N_4S_5^+$: 374.9900.

1a-S_4: Suitable crystals for X-ray diffraction were grown by liquid-liquid diffusion from $CHCl_3$ and hexanes; m.p. > 240 °C; ^{1}H NMR (500 MHz, $CDCl_3$): δ_H 4.25 (s, 6H), 4.05 (s, 6H); ^{13}C NMR (126 MHz, $CDCl_3$): δ_C 177.7, 172.7, 145.3, 123.8, 43.9, 43.6. IR (ATR): $\tilde{\nu}$ = 2928 (w), 1524 (s, C=C), 1416 (s, sh at 1472 cm^{-1}), 1280 (s, sh at 1248 cm^{-1}, ring motion involving C=S), 1167 (m, ring motion involving C=S), 1081 (s), 1064 (s), 993 (w), 872 (w), 812 (w), 666 (m), 606 (m) cm^{-1}; HR-MS (ES+): 372.9743 *m/z* ([*M* + H]$^+$), calcd for $C_{12}H_{13}N_4S_5^+$: 372.9744).

Optimized Synthesis for 1a-S_4 and 1b-S_4

A mixture of *N,N'*-dimethyl-2-thiobarbituric acid (100 mg, 0.58 mmol) or *N,N'*-diethyl-2-thiobarbituric acid (110 mg, 0.54 mmol), Lawesson's reagent (0.5 eq) and anhydrous toluene (10 mL per 100 mg of *N,N'*-dialkylbarbituric acid) was irradiated at 365 nm and stirred at reflux for 24 h. The reaction was then cooled to r.t., and the reaction mixture was washed with sat. $NaHCO_3$ (100 mL) and extracted with CH_2Cl_2. The organic layers were collected, dried over Na_2SO_4 and the solvent was removed under vacuum. The crude mixture was purified by silica gel chromatography (1:1, CH_2Cl_2: toluene) to give **1a-S_4** (48 mg, 44%) as a red solid or **1b-S_4** (65 mg, 60%) as a red solid.

1b-S_4: suitable crystals for X-ray diffraction were grown by liquid-liquid diffusion from $CHCl_3$ and hexanes; m.p. 217–219 °C; ^{1}H NMR (500 MHz, $CDCl_3$): δ_H 5.14 (d, *J* 6.5 Hz, 4H), 4.57 (q, *J* = 7.1 Hz, 4H), 1.52 (t, *J* = 7.1 Hz, 6H), 1.45 (q, *J* = 6.5 Hz, 6H); ^{13}C NMR (126 MHz, $CDCl_3$): δ_C 176.3, 171.1, 144.7, 124.1, 52.1, 50.4, 12.0, 11.1; IR (ATR): $\tilde{\nu}$ = 2965 (w), 2926 (w), 1703 (w), 1522 (s, C=C), 1445 (m), 1356 (s, sh at 1368 cm^{-1}), 1248 (s, sh at 1162 cm^{-1}, ring motion involving C=S), 1098 (s), 923 (w), 868 (m), 796 (w), 759 (w), 687 (m) cm^{-1}; HR-MS (ES+): 429.0370 *m/z* ([M + H])$^+$, calcd for $C_{16}H_{21}N_4S_5^+$ = 429.0364.

Synthesis of 6, 2a-O_2S_2, and 2b-O_2S_2

A mixture of *N,N'*-dimethylbarbituric acid (100 mg, 0.63 mmol) or *N,N'*-diethylbarbituric acid (100 mg, 0.55 mmol), Lawesson's reagent (2.5 eq) and anhydrous toluene (10 mL) was irradiated at 365 nm and stirred at reflux for 24 h. The reaction was then cooled to r.t., and the reaction mixture was washed with sat. $NaHCO_3$ solution, H_2O and then extracted with CH_2Cl_2. The organic layers were dried over Na_2SO_4 and the organic solvents were removed under vacuum. The mixture was purified using silica gel chromatography (100% CH_2Cl_2) to give **6** (19 mg, 16%) as a yellow solid, **2a-O_2S_2** (72 mg, 67%) as a red solid, or **2b-O_2S_2** (24 mg, 22%) as a red solid.

The structural characterization data for **6** are in agreement with the literature; m.p. 194–197 °C, literature m.p. 196 °C.[22]

2a-O_2S_2: Suitable crystals for X-ray diffraction were grown by slow evaporation from $CHCl_3$; m.p. > 240 °C; ^{1}H NMR (500 MHz, $CDCl_3$): δ_H 3.80 (s, 6H), 3.61 (s, 6H); ^{13}C NMR (126 MHz, $CDCl_3$): δ_C 180.7, 148.8, 145.2, 121.0, 35.8, 35.6; IR (ATR): $\tilde{\nu}$ = 1682 (s, C=O), 1551 (m, C=C), 1534 (m, C=C), 1444 (m, sh at 1401 cm^{-1}), 1285 (m, ring motion involving C=S), 1192 (w), 1114 (m, sh at 1058 cm^{-1}), 1010 (w), 965 (w), 832 (w), 733 (s), 700 (s), 665 (w) cm^{-1}; HR-MS (ES+): 341.0200 *m/z* ([M + H])$^+$, calcd for $C_{16}H_{21}N_4O_2S_3^+$ = 341.0195.

2b-O_2S_2: M.p. 231–234 °C; ^{1}H NMR (500 MHz, $CDCl_3$): δ_H 4.56 (q, *J* = 7.0 Hz, 4H), 4.02, (q, *J* = 7.2 Hz, 4H), 1.42 (t, *J* = 7.2 Hz, 6H), 1.34 (t, *J* = 7.0 Hz, 6H); ^{13}C NMR (126 MHz, $CDCl_3$): δ_C 179.8, 147.7, 144.5, 121.4, 45.3, 43.4, 13.1, 12.0; IR (ATR): $\tilde{\nu}$ = 2978 (w), 1678 (s, C=O), 1539 (m, C=C), 1434 (m, sh at 1479 cm^{-1}), 1337 (w), 1244 (m, ring motion involving C=S), 1127 (m), 1089 (m), 1032 (w), 830 (w), 786 (w), 741 (s), 658 (w) cm^{-1}; HR-MS (ES+): 341.0200 *m/z* ([M + H]$^+$), calcd for $C_{16}H_{21}N_4O_2S_3^+$ = 341.0195.

Synthesis of 3a-OS_3

A mixture of **1a-S_4** (48 mg, 0.13 mmol), CuCl (50 mg, 0.50 mmol), 10% NaOH solution (2 mL) and MeCN (4 mL) were stirred at r.t. for 24 h. The reaction mixture was then washed with H_2O and extracted with CH_2Cl_2. The organic layers were collected, dried over Na_2SO_4 and the solvent was removed under vacuum to give **3a-OS_3** (46 mg, quant.) an orange solid. Suitable crystals for X-ray diffraction were grown by liquid-liquid diffusion from $CHCl_3$ and toluene; m.p. > 240 °C; ^{1}H NMR (500 MHz, $CDCl_3$): δ_H 4.26 (s, 3H), 4.04 (s, 3H), 4.03 (s, 3H), 3.84 (s, 3H); ^{13}C NMR (126 MHz, $CDCl_3$): δ_C 179.9, 175.4, 172.9, 153.4, 149.2, 143.1, 124.3, 113.5, 44.6, 44.0, 43.0, 36.7. IR (ATR): $\tilde{\nu}$ = 2922 (w), 2849 (w), 1697 (s, C=O), 1524 (m, C=C), 1416 (m, sh at 1472 cm^{-1}), 1292 (m, ring motion involving C=S), 1126 (m, ring motion involving C=S), 1061 (m), 1001 (w), 907 (m), 834 (w), 756 (m), 696 (m) cm^{-1}; HR-MS (AP+): 356.9972 *m/z* ([*M* + H]$^+$), calcd for $C_{12}H_{13}N_4OS_4^+$: 356.9967).

Synthesis of 4a-O_4 and 3b-OS_3

A mixture of **3a-OS_3** (40 mg, 0.11 mmol) or **1b-S_4** (180 mg, 0.45 mmol), CuCl (4 eq), 10% NaOH solution (1.5 mL per 50 mg of **3a-OS_3** or **1b-S_4**) and MeCN (4 mL per 50 mg of **3a-OS_3** or **1b-S_4**) were stirred at reflux for 24 h. The reaction was then cooled to r.t., and the reaction mixture was washed with H_2O and extracted with CH_2Cl_2. The organic layers were collected, dried over Na_2SO_4 and the solvent was removed under vacuum to give **4a-O_4** (28 mg, 75%) as a white solid or **3b-OS_3** (45 mg, 24%) as a yellow solid.

4a-O_4: Suitable crystals for X-ray diffraction were grown by liquid-liquid diffusion from $CHCl_3$ and hexanes; m.p. > 240 °C; ^{1}H NMR (500 MHz, $CDCl_3$): δ_H 3.59 (s, 6H), 3.45 (s, 6H); ^{13}C NMR (126 MHz, $CDCl_3$): δ_C 156.0, 150.6, 146.9, 110.8, 35.0, 29.1; IR (ATR): $\tilde{\nu}$ = 2922 (m, sh at 2851 cm^{-1}), 1700 (s, sh at 1738 cm^{-1}, C=O), 1655 (s, C=O), 1562 (s, C=C), 1462 (s, sh at 1424 cm^{-1}), 1242 (m, br), 1096 (m), 1020 (m), 986 (m), 908 (m), 874 (m), 800 (m), 737 (s) cm^{-1}; HR-MS (ES+): 309.0653 *m/z* ([M + H]$^+$), calcd for $C_{12}H_{13}N_4O_4S^+$ = 309.0652.

3b-OS_3: M.p. 200–202 °C; ^{1}H NMR (500 MHz, $CDCl_3$): δ_H 5.14 (m, 2H), 4.66–4.53 (m, 6H), 1.49 (dt, *J* = 11.0, 7.1 Hz, 6H), 1.44 (t, *J* = 6.9 Hz, 3H), 1.34 (t, *J* = 7.0 Hz, 3H); ^{13}C NMR (126 MHz, $CDCl_3$): δ_C 178.4, 174.0, 171.4, 152.9, 148.4, 142.4, 124.5, 144.0, 52.4, 51.3, 50.9, 44.8, 11.9, 11.7, 11.6, 10.7; IR (ATR): $\tilde{\nu}$ = 2982 (w), 2936 (w), 1695 (s, C=O), 1520 (m, C=C), 1437 (m), 1333 (m, sh at 1378 cm^{-1}), 1237 (s, sh at 1204 cm^{-1}, ring motion involving C=S), 1126 (m, ring motion involving C=S), 1076 (m), 974 (m), 835 (w), 743 (m), 704 (m) cm^{-1}; HR-MS (ES+): 413.0595 *m/z* ([M + H]$^+$), calcd for $C_{16}H_{21}N_4OS_4^+$ = 413.0593.

Single-Crystal X-Ray Data

Deposition Numbers 2244092 (for **1a-S_4**), 2244099 (for **2a-O_2S_2**), 2251143 (for **3a-OS_3**), 2247147 (for **4a-O_4**), 2246037 (for **1b-S_4**), and 2244101 (for **5**) contain the supplementary crystallographic data for this paper. These data are provided free of charge by the joint Cambridge Crystallographic Data Centre and Fachinformationszentrum Karlsruhe Access Structures service **www.ccdc.cam.ac.uk/structures**.

Acknowledgements

Part of this research was undertaken using the supercomputing facilities at Cardiff University operated by Advanced Research Computing at Cardiff (ARCCA) on behalf of the Cardiff Supercomputing Facility and the HPC Wales and Supercomputing Wales (SCW) projects. We acknowledge the support of the latter, which is part-funded by the European Regional Development Fund (ERDF) via the Welsh Government. We thank the financial support from the School of Chemistry at Cardiff University and the UK Engineering and Physical Sciences Research Council (EPSRC) through grants EP/W03431X/1. A.I.W. is supported by EPSRC through Doctoral Training Partnerships (DTP).

Supplementary Material

Copies of single-crystal X-ray structures, calculated cartesian coordinates, additional electron spin density plots, and ^{1}H NMR, ^{13}C NMR and IR spectra of all new compounds are given in the Supplementary Material file associated with this manuscript.

References

1. Iijima, K.; Le Gal, Y.; Higashino, T.; Lorcy, D.; Mori, T. *J. Mater. Chem. C* **2017**, *5*, 9121. https://doi.org/10.1039/C7TC02886E
2. Yi, W.; Zhao, S.; Sun, H.; Kan, Y.; Shi, J.; Wan, S.; Li, C.; Wang, H. *J. Mater. Chem. C* **2015**, *3*, 10856. https://doi.org/10.1039/C5TC02287H
3. Filatre-Furcate, A.; Higashino, T,; Lorcy, D.; Mori, T. *J. Mater. Chem. C* **2015**, *3*, 3569. https://doi.org/10.1039/C5TC00253B
4. Lv, W.; Yang, B.; Wang, B.; Wan, W.; Ge, Y.; Yang, R.; Hao, C.; Xiang, J.; Zhang, B.; Zeng, Z.; Liu, Z. *ACS Appl. Mater. Interfaces* **2018**, *10*, 9663. https://doi.org/10.1021/acsami.7b19169
5. Dang, D.; Zhou, P.; Wu, Y.; Xu, Y.; Zhi, Y.; Zhu, W. *Phys. Chem. Chem. Phys.* **2018**, *20*, 13171. https://doi.org/10.1039/C7CP08567B
6. Wang, C.; Abbas, M.; Wantz, G.; Kawabata, K.; Takimiya, K. *J. Mater. Chem. C* **2020**, *8*, 15119. https://doi.org/10.1039/D0TC01408G
7. Lévesque, S.; Gendron, D.; Bérubé, N.; Grenier, F.; Leclerc, M.; Coîté, M. *J. Phys. Chem. C* **2014**, *118*, 3953. https://doi.org/10.1021/jp411300h

8. Yang, T. F.; Huang, S. H.; Chiu, Y. P.; Chen, B. H.; Shih, Y. W.; Chang, Y. C.; Yao, J. Y.; Lee, Y. J.; Kuo, M. Y. *Chem. Commun.* **2015**, *51*, 13772. https://doi.org/10.1039/C5CC04674B
9. Tilley, A. J.; Guo, C.; Miltenburg, M. B.; Schon, T. B.; Yan, H.; Li, Y.; Seferos, D. S. *Adv. Funct. Mater.* **2015**, *25*, 3321. https://doi.org/10.1002/adfm.201500837
10. Silaghi-Dumitrescu, R.; Lupan, A. *Cent. Eur. J. Chem.* **2013**, *11*, 457. https://doi.org/10.2478/s11532-012-0178-z
11. Antonijević, I. S.; Janjić, G. V.; Milčić, M. K.; Zarić, S. D. *Cryst. Growth Des.* **2016**, *16*, 632. https://doi.org/10.1021/acs.cgd.5b01058
12. Ando, S.; Nishida, J.; Tada, H.; Inoue, Y.; Tokito, S.; Yamashita, Y. *J. Am. Chem. Soc.* **2005**, *127*, 5336. https://doi.org/10.1021/ja042219+
13. Gendron, D.; Maasoumi, F.; Armin, A.; Pattison, K.; Burn, P. L.; Meredith, P.; Namdas, E. B.; Powell, B. J. *RSC Adv.* **2017**, *7*, 10316. https://doi.org/10.1039/C7RA00693D
14. Ryo, S.; Yoo, D.; Iijima, K.; Sato, R.; Le Gal, Y.; Lorcy, D.; Mori, T. *New. J. Chem.* **2019**, *43*, 11865. https://doi.org/10.1039/C9NJ02731A
15. Sumimoto, Y.; Iijima, K.; Yoo, D.; Kawamoto, T.; Le Gal, Y.; Lorcy, D.; Mori, T. *CrystEngComm* **2020**, 22, 6920. https://doi.org/10.1039/D0CE01133A
16. Wright, A. I.; Kariuki, B. M.; Wu, Y.-L. *Eur. J. Org. Chem.* **2021**, *2021*, 4647. https://doi.org/10.1002/ejoc.202100793
17. Palmer, J. R.; Wells, K. A.; Yarnell, J. E.; Favale, J. M.; Castellano, F. N. *J. Phys. Chem. Lett.* **2020**, *11*, 5092. https://doi.org/10.1021/acs.jpclett.0c01634
18. Chen, T. G.; Zhang, X. Q.; Ge, J. F.; Xu, Y. J.; Sun, R. *Spectrochim. Acta A Mol. Biomol. Spectrosc.* **2022**, *270*, 120783. https://doi.org/10.1016/j.saa.2021.120783
19. Taeufer, T.; Hauptmann, R.; El-Hage, F.; Mayer, T. S.; Jiao, H.; Rabeah, J.; Pospech, J. *ACS Catal.* **2021**, *11*, 4862. https://doi.org/10.1021/acscatal.0c05540
20. Petrosyan, A.; Zach, L.; Taeufer, T.; Mayer, T. S.; Rabeah, J.; Pospech, J. *Chem. Eur. J.* **2022**, *28*, e202201761. https://doi.org/10.1002/chem.202201761
21. Perregaard, J.; Scheibye, S.; Meyer, H. J.; Thomsen, I.; Lawesson, S.-O. *Bull. Soc. Chim. Belg.* **1977**, *86*, 679. https://doi.org/10.1002/bscb.19770860905
22. Mohamed, N. R. *Phosphorus Sulfur Silicon Relat. Elem.* **2000**, *161*, 123. https://doi.org/10.1080/10426500008042100
23. Narasimhamurthy, N.; Samuelson, A. G. *Tetrahedron Lett.* **1986**, *27*, 3911. https://doi.org/10.1016/S0040-4039(00)83914-3
24. Senga, K.; Ichiba. M.; Nishigaki. S. *J. Org. Chem.* **1978**, *43*, 1677. https://doi.org/10.1021/jo00403a012
25. Steer, R. P.; Ramamurthy, V. *Acc. Chem. Res.* **1988**, *21*, 380. https://doi.org/10.1021/ar00154a005
26. Maciejewski, A.; Steer, R. P. *Chem. Rev.* **1993**, *93*, 67.

https://doi.org/10.1021/cr00017a005
27. Coyle, J. D. *Tetrahedron* **1985**, *41*, 5393. https://doi.org/10.1016/S0040-4020(01)91341-9
28. Sumathi, K.; Chandra, A. K. *J. Photochem. Photobiol. A Chem.* **1988**, *43*, 313. https://doi.org/10.1016/1010-6030(88)80028-5
29. Itoh, T.; Ogura, H.; Watanabe, K. A. *Tetrahedron Lett.* **1977**, *18*, 2595. https://doi.org/10.1016/S0040-4039(01)83829-6
30. Schultz, A. G.; DeTar, M. B. *J. Am. Chem. Soc.* **1976**, *98*, 3564. https://doi.org/10.1021/ja00428a029
31. Groen, S. H.; Kellogg, R.M.; Buter, J.; Wynberg, H. *J. Org. Chem.* **1968**, *33*, 2218. https://doi.org/10.1021/jo01270a011
32. Schultz, A. G.; DeTar, M. B. *J. Am. Chem. Soc.* **1974**, *96*, 296. https://doi.org/10.1021/ja00808a071
33. Paulini, R.; Müller, K.; Diederich, F. *Angew. Chem. Int. Ed.* **2005**, *44*, 1788. https://doi.org/10.1002/anie.200462213
34. Newberry, W.; Vanveller, B.; Guzei, I. A.; Raines, R. T. *J. Am. Chem. Soc.* **2013**, *135*, 7843. https://doi.org/10.1021/ja4033583
35. Pascoe, D. J.; Ling, K. B.; Cockroft, S. L. *J. Am. Chem. Soc.* **2017**, *139*, 15160. https://doi.org/10.1021/jacs.7b08511
36. Gaussian 09, Revision D.01, Frisch, M.J.; Trucks, G.W.; Schlegel, H.B.; Scuseria, G.E.; Robb, M.A.; Cheeseman, J.R.; Scalmani, G.; Barone, V.; Mennucci, B.; Petersson, G.A.; Nakatsuji, H.; Caricato, M.; Li, X.; Hratchian, H.P.; Izmaylov, A.F.; Bloino, J.; Zheng, G.; Sonnenberg, J.L.; Hada, M.; Ehara, M.; Toyota, K.; Fukuda, R.; Hasegawa, J.; Ishida, M.; Nakajima, T.; Honda, Y.; Kitao, O.; Nakai, H.; Vreven, T.; Montgomery, J.A., Jr.; Peralta, J.E.; Ogliaro, F.; Bearpark, M.; Heyd, J.J.; Brothers, E.; Kudin, K.N.; Staroverov, V.N.; Kobayashi, R.; Normand, J.; Raghavachari, K.; Rendell, A.; Burant, J.C.; Iyengar, S.S.; Tomasi, J.; Cossi, M.; Rega, N.; Millam, N.J.; Klene, M.; Knox, J.E.; Cross, J.B.; Bakken, V.; Adamo, C.; Jaramillo, J.; Gomperts, R.; Stratmann, R.E.; Yazyev, O.; Austin, A. J.; Cammi, R.; Pomelli, C.; Ochterski, J. W.; Martin, R.L.; Morokuma, K.; Zakrzewski, V.G.; Voth, G.A.; Salvador, P.; Dannenberg, J.J.; Dapprich, S.; Daniels, A.D.; Farkas, Ö.; Foresman, J.B.; Ortiz, J.V.; Cioslowski, J.; Fox, D.J. Gaussian, Inc., Wallingford CT, **2009**.
37. Wu, Y.-L.; Wright, A. I. *Phys. Chem. Chem. Phys.* **2023**, *25*, 1342. https://doi.org/10.1039/D2CP05186A
38. Alvarez, S. *Dalton Trans.* **2013**, *42*, 8617. https://doi.org/10.1039/c3dt50599e
39. Prasanthkumar, K. P.; Suresh, C. H.; Aravindakumar, C. T. *J. Org. Phys. Chem.* **2013**, *26*, 510. https://doi.org/10.1002/poc.3116
40. Skotnicki, K.; Taras-Goslinska, K.; Janik, I.; Bobrowski, K. *Molecules* **2019**, *24*, 4402. https://doi.org/10.3390/molecules24234402
41. Shinde, R. G.; Khan, A. A.; Barik, A. *Free Radic. Res.* **2019**, *53*, 629. https://doi.org/10.1080/10715762.2019.1617417
42. Hendon, C. H.; Carbery, D.R.; Walsh, A. *Chem. Sci.* **2014**, *5*, 1390. https://doi.org/10.1039/C3SC53432D